Magnetic-Free Wireless Self-Direct Drive Motor System for Biomedical Applications with High-Robustness

Zhiwei Xue, *Graduate Student Member, IEEE*, K.T. Chau, *Fellow, IEEE*, Wei Liu, *Member, IEEE*, and Zhichao Hua, *Member, IEEE*

***Abstract*—The integration of high-precision robotics and magnetic resonance imaging (MRI) exhibits the potential to enhance the accuracy and safety of MRI image-guided surgery. However, the potential hazards associated with conventional electromagnetic servomotors in strong magnetic fields have hindered the development of MRI-compatible robotics. To address this issue, this paper proposes and implements a novel magnetic-free wireless drive system that creatively integrates capacitive power transfer (CPT) with ultrasonic motors (USM) to realize the truly wireless self-direct drive without strong magnetic field interference. The proposed system overcomes the drawbacks of existing wireless motors requiring microcontrollers, power switches and communication modules at the motor side, facilitating high-degree integration and maintenance-free operation. In addition, a dual-mode wireless drive control scheme is proposed to achieve the full-speed range wireless direct drive. Promisingly, the proposed system is unaffected by coupling mechanism misalignment and load variation, ensuring precise manipulation with high robustness. Both theoretical analysis and experimental results are conducted to verify the effectiveness of the proposed wireless motor system.**

***Index Terms*—Wireless power transfer, ultrasonic motors, high-robustness, biomedical application.**

I. INTRODUCTION

Wireless power transfer (WPT), as a non-contact electric power transmission technology, exhibits the obvious advantages of flexibility, convenience, and safety [1], [2]. In recent years, WPT has shown great potential in numerous emerging areas such as wireless energy routers [3], electric vehicles [4], [5], and medical implants [6].

Notably, WPT has been increasingly applied to motor drives with the advantages of no messy wires and electric shock risk [7], [8]. In [9], a wireless in-wheel motor system was developed to remove the power supply cables exposed to harsh environments. However, only the power transfer method is changed to wireless, the controller and power converters are still required at the motor side, which undoubtedly increases the maintenance requirements. To improve the reliability of the system, wireless motor systems without controller and power converters at the motor side is highly desirable.

Recently, a wireless DC motor system with bidirectional motion capabilities was developed by inducing bipolar voltages on the motor windings through selective inductive power transfer [10]. However, the carbon brushes and commutators of DC motors require regular maintenance, which inevitably increases the safety considerations. On the other hand, wireless shaded-pole induction motors (SPIMs) have been developed for their high robustness without carbon brushes and commutators [11], but this system inevitably requires numerous active power switches at the motor side, increasing the risk of failure in confined environments [12].

In addition, wireless switched reluctance motors (SRMs) have been developed by using multiple receivers with different resonant frequencies to selectively excite the corresponding motor windings [13], but the coupling mechanism and switched capacitor arrays make the system clumsy and complex [14]. On the other hand, the wireless SRM system with constant resonant frequency was developed to drive the SRM directly through a single power transfer channel [15], which improved the integration and compactness. In [16], a wireless stepping motor utilized multi-channel WPT to wirelessly excite the motor windings separately to realize precise position control. However, the essential Bluetooth communication device and multiple rectifiers for wireless SRMs and stepping motors increase the concerns of the maintenance-free operation and cost of the system [17].

It should be noted that the above wireless motor systems can be controlled entirely at the primary side, but active or passive power switches and communication modules are inevitably required at the motor side, which increases the risk of failure due to complexity. In addition, the existing wireless motors mainly focus on speed and power control and underperform in robustness to coupling mechanism misalignment, which limits their practical applications in complex operating environments [18]. Moreover, they are extremely sensitive to high magnetic field interference and cannot meet the requirements of biomedical applications associated with strong magnetic fields [19].

Manuscript received July 10, 2023; revised October 03, 2023; accepted November 12, 2023. This work was partially supported by a grant from the Hong Kong Research Grants Council, Hong Kong Special Administrative Region, China, under Project No. T23-701/20-R, and partially supported by a grant from The Hong Kong Polytechnic University, under Project No. P0048560. *(Corresponding author: K.T. Chau)*

Z. Xue and Z. Hua are with the Department of Electrical and Electronic Engineering, The University of Hong Kong, Hong Kong, China. (e-mail: zwxue@eee.hku.hk; zchua@eee.hku.hk).

K.T. Chau and W. Liu are with the Research Centre for Electric Vehicles and Department of Electrical and Electronic Engineering, The Hong Kong Polytechnic University, Hong Kong, China. (e-mail: k.t.chau@polyu.edu.hk; wei.liu@polyu.edu.hk)

Therefore, a novel magnetic-free wireless self-direct drive ultrasonic motors (USM) system with high-robustness is proposed in this paper. The proposed system can operate in the non-magnetic state, which is attractive for magnetic resonance imaging (MRI)-compatible surgical robots, as shown in Fig. 1. The absence of wires or cables avoids the risk of injury to patients or technicians due to wire movement during scanning, making the proposed system compatible with MRI scanners and more flexible in placement. Promisingly, with the proposed dual-mode wireless drive control, the bidirectional motion capability and precise positioning can be readily achieved at the primary side without the need for complex peripheral circuits or multi-frequency WPT, enabling innovative wireless self-direct drive. Notably, the proposed system is insensitive to the misalignment of the coupling mechanism, overcoming the drawbacks of existing wireless motors with insufficient robustness, which improves adaptability under complex operating conditions.

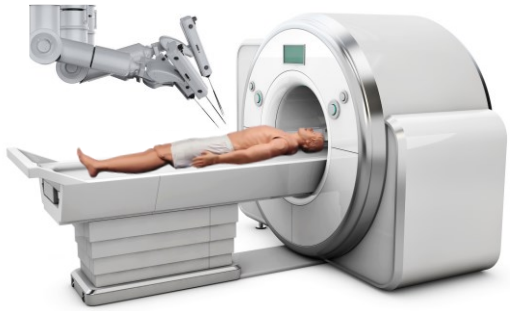

Fig. 1. Schematic of MRI-compatible surgical robot.

In Section II, the configuration of the proposed wireless USM and the comparison with existing wireless motor systems are conducted. Then, the working principles of USM are described in Section III. Section IV is the design of the proposed system. Section V will give the implementation and experimental results to verify the feasibility of the proposed system. Finally, conclusions will be drawn in Section VI.

II. System Design and Analysis

A. Configuration of Proposed Magnetic-Free Wireless Self-Direct Drive Motor System

The configuration of the proposed magnetic-free wireless self-direct drive USM is shown in Fig. 2, which comprises a high-frequency inverter, double-T resonant networks, and a USM. Unique from existing wireless motor systems, the proposed system can directly drive the USM through the secondary T-type resonant networks without needing any power switches or communication modules.

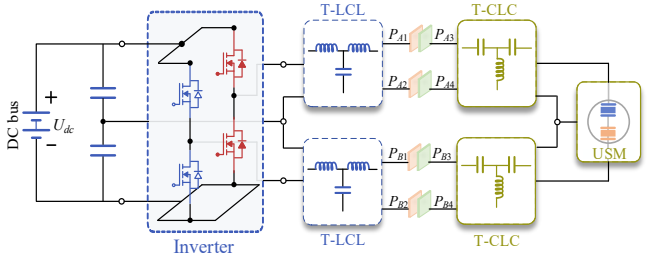

Fig. 2. Configuration of proposed wireless self-direct drive USM.

In addition, the insensitivity to the misalignment of the coupling mechanism is another definite advantage of the proposed system over other wireless motors. Specifically, the performance of existing wireless motors is heavily reliant on the alignment of the coupling mechanism, which limits their applicability in complex operating conditions. In contrast, the proposed system is insensitive to the misalignment of the coupling mechanism, and the variation of the mutual capacitance will not affect the control and operation of the motor. Therefore, the proposed wireless USM represents a promising solution to the drawbacks of existing wireless motors in terms of the requirements of multiple power switches and insufficient robustness.

B. Comparison of Existing Wireless Motor Systems

The wireless permanent magnet (PM) DC motors have been widely researched due to their straightforward operating principles [20], as shown in Fig. 3(a), where high-frequency AC power is transferred wirelessly from the primary side to the secondary side, and then fed to the DC motor through the secondary rectifier and filter capacitor.

Conversely, the wireless AC motor presents a more intricate driver system in comparison to the DC counterpart, as the wireless SPIM with full-bridge inverters has been investigated, where numerous active and passive power switches are required. Although the wireless SPIM using half-bridge inverters with fewer active power switches has been developed as shown in Fig. 3(b), this structure is only applicable to SPIMs with dual-stator windings.

The multi-frequency-based wireless SRM system depicted in Fig. 3(c) employs a multi-frequency compensation network, enabling the single transmitter to provide multi-frequency power to three receivers with different resonant frequencies and finally to feed motor three-phase via rectifiers. Moreover, Bluetooth technology is commonly used to establish wireless communication of the rotor position to the primary controller, which increases concerns about EMI suppression.

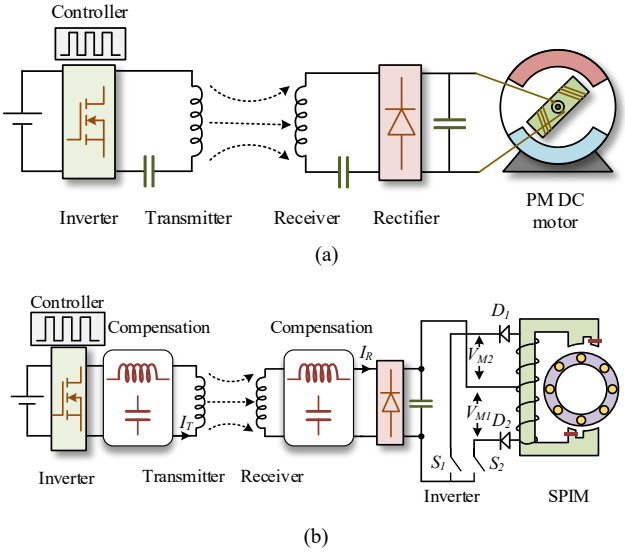

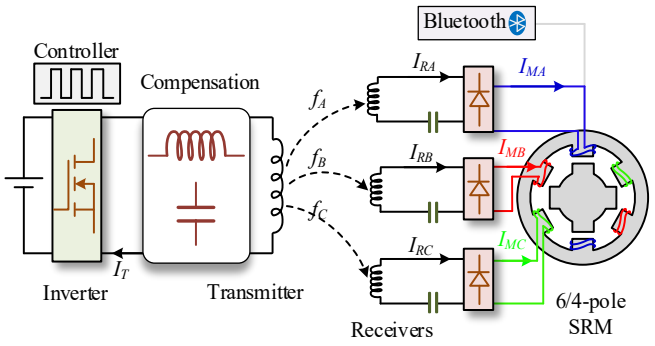

(c)

Fig. 3. Configuration comparison of existing wireless motor systems. (a) Wireless DC motor system [20]. (b) Wireless SPIM system [12]. (c) Multi-frequency wireless SRM system [13].

Although existing wireless motors can implement servo control at the primary side, complex peripheral circuits, active power switches, multiple rectifiers and communication devices are unavoidably required at the motor side, which inevitably reduces the simplicity and reliability. In addition, robustness is a tricky issue worth considering for wireless motor systems, as misalignment of the coupling mechanisms can seriously affect the viability of existing wireless motors.

Therefore, in response to the above problems, the distinct contributions and innovations of the proposed wireless USM can be summarized as follows:

1. Wireless self-direct drive of the proposed wireless USM can be readily achieved by the secondary T-type resonance network without complex peripheral circuits, microcontrollers, power switches, and communicators at the motor side.

2. The proposed system exhibits a high degree of robustness in the face of coupling mechanism misalignment, thanks to its ability to guarantee a stable and consistent power supply regardless of coupling mechanism misalignment and load variations.

3. This system is impervious to potential disruption from strong-magnetic-fields, which is conducive to strong-magnetic-field applications.

4. Accurate positioning and motion control can be readily achieved as the full-speed-range bidirectional motion capability can be easily implemented at the primary side with the proposed dual-mode wireless drive control.

5. The elimination of additional devices at the motor side and the maintenance-free feature of the USM without carbon brushes and commutator make the proposed system more cost-effective for promotion and commercialization.

III. Working Principles of USM

The operating principles of the USM diverge from those of traditional electromagnetic motors [21], owing to its utilization of the piezoelectric effect and ultrasonic vibration [22]. As shown in Fig. 4, two sets of piezoelectric elements are placed in the appropriate positions and driven by two voltage sources A and B, respectively. When the piezoelectric elements are excited by the high-frequency voltage, a traveling wave propagating along the stator is generated. Then, a tangential force will be induced by the frictional coupling between the stator and rotor to drive the rotor in the direction opposite to the traveling wave, realizing the conversion of electrical energy to mechanical energy. In addition, the direction of the traveling waves depends on which voltage source is leading in phase. Specifically, when the A-phase voltage source leads the B-phase, the traveling wave will move to the right, and vice versa [23]. Therefore, by appropriately setting the phase difference between voltage sources, motor commutation control can be readily realized.

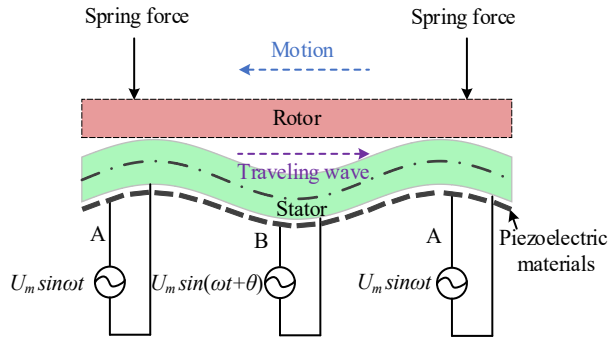

Fig. 4. Operating principle of USM.

IV. Design of Wireless Self-Direct Drive Motor System

The performance of existing wireless motor systems relies heavily on the matching degree of the coupling mechanism, the misalignment of the coupling mechanism will seriously impair the viability of the whole system. Therefore, it is critical to develop a robust and reliable wireless motor that is insensitive to the misalignment of the coupling mechanism. In addition, since USMs exhibit strong nonlinear behavior, with their equivalent impedance varying with the mechanical, electrical and thermal properties, the constant voltage output characteristic independent of the load impedance is crucial to ensure their steady operation. To this end, a double-T resonant network capacitive power transfer (CPT) system with coupling capacitance-independent as well as load-independent constant voltage output characteristics is developed and analyzed to meet the demanding requirements of the wireless USM drive.

A. Design of Coupling Mechanism Independent Constant-Current Output

Fig. 5 shows the schematic of the double-T resonant network CPT system, where two inductors L_{p1} and L_{p2}, together with a resonant capacitor C_p form the primary T-type LCL resonant network, while C_{s1}, C_{s2}, and L_s form the secondary T-type CLC resonant network. The capacitive coupling mechanism is composed of two pairs of metal plates and the equivalent coupling model is shown in Fig. 6.

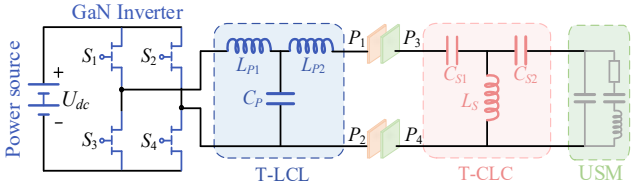

Fig. 5. Schematic of double-T resonant network CPT system for single-phase USM stator.

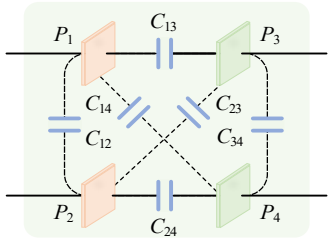

Fig. 6. Circuit model of coupling mechanism.

It can be observed that 6 coupling capacitors are induced between any two of the four coupling plates [24]. In this work, water is placed in the coupling mechanisms to increase the coupling capacitance and transmission power. Therefore, the capacitances C_{12} and C_{34}, as well as the cross-coupling capacitances C_{14} and C_{23}, can be ignored as they are much smaller than C_{13} and C_{24} [25]. Therefore, the coupling mechanisms can be simplified as

$$C_M = \frac{C_{13}C_{24}}{C_{13}+C_{24}} \tag{1}$$

Accordingly, the equivalent circuit of the proposed double-T type CPT system is shown in Fig. 7, where the model of single-phase USM is represented by Z_L for convenience.

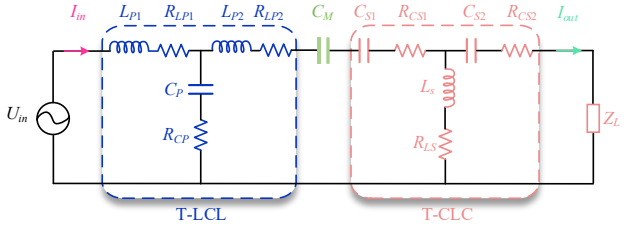

Fig. 7. Equivalent circuit of double-T type CPT system.

To ensure that the coupling capacitance C_M has minimal impact on the WPT, it is crucial to design the primary T-resonant network with constant current output characteristics. Specifically, by ensuring that the output current of the primary T-resonant network resembles the output of a current source, the transmission current is less affected by the variation of C_M. Fig. 8 depicts the simplified diagram of the primary T-LCL network.

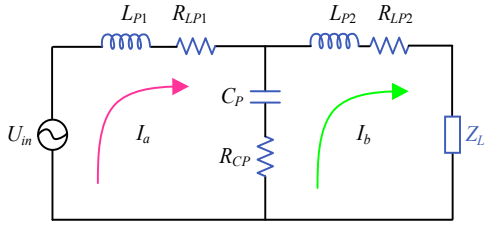

Fig. 8. Equivalent circuit of primary T-LCL structure.

According to Kirchhoff's voltage law [26], the mathematical model of the circuit shown in Fig. 8 can be expressed as

$$\begin{cases} (Z_{LP1}+Z_{CP})\dot{I}_a - Z_{Cp}\dot{I}_b = \dot{U}_{in} \\ -Z_{CP}\dot{I}_a + (Z_{LP2}+Z_{CP}+Z_L)\dot{I}_b = 0 \end{cases} \tag{2}$$

where $Z_{LP1}=R_{LP1}+j\omega L_{P1}$, $Z_{LP2}=R_{LP2}+j\omega L_{P2}$ and $Z_{CP}=R_{CP}+1/j\omega C_P$ are the impedances of inductors and capacitor, respectively.

When the T-LCL network meets the following conditions

$$L_{P1} = L_{P2} = \frac{1}{\omega^2 C_P} \tag{3}$$

The output current of the network can be derived as

$$\dot{I}_b = \frac{-Z_{CP}\dot{U}_{in}}{(R_{LP1}+R_{CP})(R_{LP2}+R_{CP})-Z_{CP}^2} \tag{4}$$

Accordingly, if the equivalent series resistances of the compensating elements are small enough, the output current can be further simplified to

$$\dot{I}_b \approx \frac{\dot{U}_{in}}{Z_{CP}} \approx \dot{U}_{in}\, j\omega C_P \tag{5}$$

From (5), when the system parameters satisfy the restrictive conditions, the output current of the network is only related to the input voltage U_{in}, the capacitance C_P and the angular frequency ω. Therefore, the designed T-LCL compensation network exhibits a constant current output independent of the rear circuit.

B. Design of Load Independent Constant-Voltage Output

According to the analysis in Section IV.*A*, the secondary T-CLC network can be considered powered by a current source, considering the primary T-type network exhibits a constant-current output, as shown in Fig. 9.

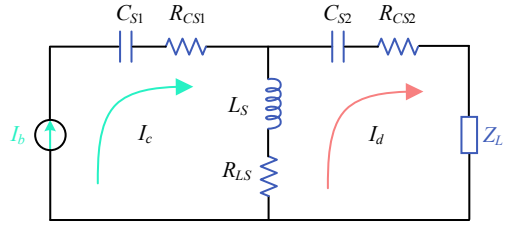

Fig. 9. Equivalent circuit of secondary T-CLC structure.

According to Kirchhoff's voltage law, the T-CLC network under the constant-current source can be expressed as

$$\begin{cases} \dot{I}_c = \dot{I}_b \\ -Z_{LS}\dot{I}_c + (Z_{LS}+Z_{CS2}+Z_L)\dot{I}_d = 0 \end{cases} \tag{6}$$

The output voltage of the T-CLC network can be derived as

$$\dot{V}_{out} = \frac{Z_{LS}Z_L\dot{I}_b}{(R_{LS}+R_{CS2}+Z_L)} \tag{7}$$

To ensure the constant-voltage output independent of load variation, the components of the T-CLC network should meet the following conditions

$$C_{S1} = C_{S2} = \frac{1}{\omega^2 L_S} \tag{8}$$

$$\begin{cases} R_{LS} \ll \omega L_S \\ R_{CS2} \ll \dfrac{1}{\omega C_{S2}} \\ (R_{LS}+R_{CS}) \ll Z_L \end{cases} \tag{9}$$

Accordingly, the output voltage can be simplified as

$$\dot{V}_{out} \approx Z_{LS}\dot{I}_b \approx j\omega L_S \dot{I}_b \tag{10}$$

It can be deduced from (10) that the output voltage of the secondary T-CLC network is approximately constant, which is only determined by the input current and the compensation inductance L_S.

C. System Characteristic Analysis

The proposed double T-type CPT system can achieve a constant voltage output independent of coupling capacitance and load variations, providing a stable and constant power supply for the flexible control of wireless USM. The primary T-LCL resonant network provides a constant current supply to the secondary circuit, thus attenuating the effects of coupling capacitance and load variations. Then, the secondary T-CLC network converts the received power into constant voltage output independent of the nonlinearity of USM operation.

In addition, the proposed double T-type CPT system provides a high degree of freedom for the output voltage regulation. According to (5) and (10), the output voltage of the designed double T-type network can be derived as

$$\dot{V}_{out} = j\omega L_S \dot{I}_b = \frac{\dot{U}_{in}\, j\omega C_P}{j\omega C_S} = \dot{U}_{in}\frac{C_P}{C_S} \tag{11}$$

It can be seen that the output voltage only depends on the input voltage U_{in} and the ratio of capacitors C_P and C_S. Therefore, different output voltage requirements can be flexibly achieved by designing different capacitor ratios in the proposed double T-type CPT system.

D. Dual-Mode Wireless Drive Control

The attainment of precise manipulation and locomotion of MRI-compatible robotics necessitates the flexible control of the wireless USM. However, the general voltage-speed control cannot achieve wireless direct drive over the full-speed range due to the presence of a low-speed dead zone in the voltage control mode [27], which limits the low-speed performance of the USM. Therefore, a dual-mode wireless drive control with variable frequency (VF) control in the low-speed region and voltage amplitude control in the high-speed region is proposed to achieve fully autonomous and full-range speed regulation of wireless USM at the transmitter side, thus satisfying diverse prerequisites for MRI image-guided surgery.

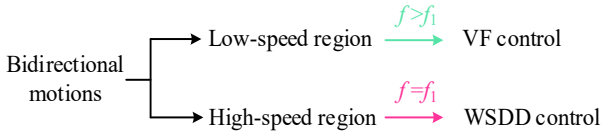

Fig. 10. Dual-mode wireless drive control scheme.

The proposed dual-mode wireless drive control scheme is shown in Fig. 10. In the low-speed region, by changing the frequency of the voltage, the wireless USM can reach a lower speed, thus overcoming the problem of the low-speed dead zone. Furthermore, to accommodate high-speed operation, a wireless self-direct drive (WSDD) scheme is developed, which can achieve the flexible regulation of the high-frequency voltage amplitude with a low switching frequency.

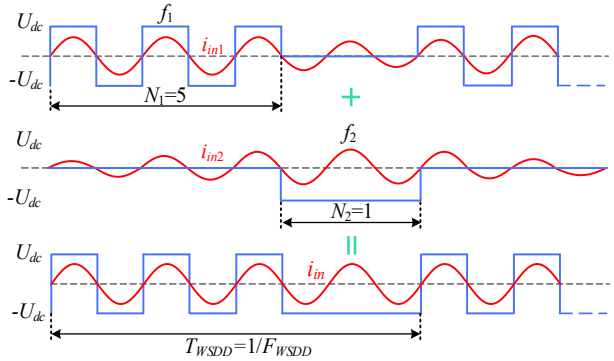

Fig. 11. Basic principle of WSDD control.

The basic principle of WSDD control is shown in Fig. 11, where N_1 and N_2 are the numbers of modulated square waves with switching frequencies f_1 and f_2, respectively. In this work, f_1 equals the resonant frequency of the double-T resonant network, and f_2 is one-third of f_1. By alternating modulation of f_1 and f_2, the inverter output can be flexibly regulated. The corresponding Fourier series expansion of the modulated square waves is deduced as [28]

$$\begin{aligned} f(t) &= a_0 + \sum_{n=1}^{\infty}(a_n\cos 2\pi nft + b_n \sin 2\pi nft) \\ &= \frac{1}{T_{WSDD}}\int_0^{T_{WSDD}} f(t)dt \\ &+ \sum_{n=1}^{\infty}\left(\frac{2}{T_{WSDD}}\int_0^{T_{WSDD}} f(t)\cos 2\pi nftdt\right)\sin 2\pi nft \\ &+ \sum_{n=1}^{\infty}\left(\frac{2}{T_{WSDD}}\int_0^{T_{WSDD}} f(t)\sin 2\pi nftdt\right)\cos 2\pi nft \end{aligned} \tag{12}$$

where $T=1/f$ is the resonant period, and $T_{WSDD}=(N_1+3N_2)T/2$ is the period of the WSDD waveform.

Accordingly, the amplitude of the fundamental component of the modulated square waves can be expressed as

$$\begin{aligned} U_{in} = b_1 &= \frac{2}{T_{WSDD}}\int_0^{T_{WSDD}} f(t)\sin 2\pi ftdt \\ &= \frac{2}{T_{WSDD}}\left(\sum_{n=1}^{N_1}\left(\int_{\frac{(n-1)T}{2}}^{\frac{nT}{2}}(-1)^{n-1}U_{dc}\sin 2\pi ftdt\right)\right. \\ &\left. + \sum_{n=N_1+1}^{N_1+N_2}\left(\int_{N_1\frac{T}{2}+(n-N_1-1)\frac{3T}{2}}^{N_1\frac{T}{2}+(n-N_1)\frac{3T}{2}}(-1)^{n-1}U_{dc}\sin 2\pi ftdt\right)\right) \\ &= \frac{2}{T_{WSDD}}U_{dc}\left(N_1\frac{T}{\pi}+N_2\frac{T}{\pi}\right) \\ &= \frac{N_1+N_2}{N_1+3N_2}\frac{4U_{dc}}{\pi} \end{aligned} \tag{13}$$

For reference, the Fourier series expansion of the half-pulses wave with switching frequency f can be expressed as

$$f(t) = \frac{4U_{dc}}{\pi}\sum_{n=1}^{\infty}\frac{1}{n}\sin 2\pi nft \tag{14}$$

The amplitude of the fundamental component of the inverter output under the half-pulses wave is [29]

$$U_{in}^{*}=\frac{4U_{dc}}{\pi} \tag{15}$$

From (13) to (15), the amplitude of the fundamental component with WSDD control can be simplified as

$$U_{in}=\frac{N_1+N_2}{N_1+3N_2}U_{in}^{*}=\delta_{WSDD}U_{in}^{*} \tag{16}$$

Therefore, the flexible output voltage regulation can be readily achieved by adjusting δ_{WSDD}, thus enabling flexible and self-direct drive of wireless USM in the high-speed range with a reduced switching frequency.

V. Implementation and Experimental Results

A. Experimental Prototype and Testing Setup

To verify the feasibility of the proposed magnetic-free wireless USM system, a prototype is constructed for experimental demonstration, as shown in Fig. 12. The design specifications and parameters are listed in Table I. All waveforms are captured and displayed by an oscilloscope Lecroy 6100A. The high-frequency inverter is populated with gallium nitride inverter GaN-GS66508B. To reduce skinning and proximity effects, the compensating inductors are wound with Litz wire and the compensating capacitors are composed of polypropylene film capacitors.

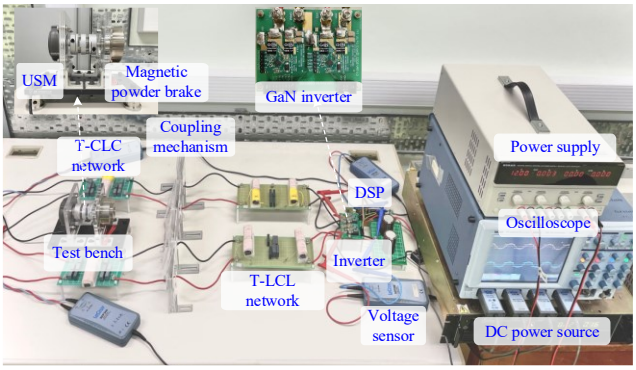

Fig. 12. Experimental setup.

TABLE I
Design Specifications and Parameters

Items	Value/type
Resonant frequency (f_1)	40 kHz
LCL inductances (L_{pA1}/L_{pA2}, L_{pB1}/L_{pB2})	4.98/4.98, 4.98/4.97 mH
LCL capacitances (C_{pA}, C_{pB})	3.18, 3.19 nF
Resistance of inductors (R_{LpA1}/R_{LpA2}, R_{LpB1}/R_{LpB2})	1.1/1.1, 1.1/1.2 Ω
CLC inductances (L_{SA}, L_{SB})	10.05, 10.03 mH
CLC capacitances (C_{SA1}/C_{SA2}, C_{SB1}/C_{SB2})	1.57, 1.58, 1.58, 1.57 nF
Resistance of inductors (R_{LSA}, R_{LSB})	1.5, 1.5 Ω
Capacitance of coupling mechanism (C_M)	1200 pF
Aluminum plate size (S)	100×100×1 mm^3
Plate distance (d)	10 mm
Rated input voltage of USM (U_n)	130 V
Microcontroller	TMS320F28335

B. Verification of Bidirectional Motions

The bidirectional motion capability of the proposed wireless USM is evaluated as shown in Fig. 13, which displays the measured waveforms of the two-phase primary-side output voltages u_{pa} and u_{pb}, and the motor terminal voltages u_{ta} and u_{tb}. The proposed system can easily achieve precise servo-control from the primary side to meet the requirements of different application scenarios. Specifically, clockwise rotation can be achieved for forward motion when A-phase voltage is ahead of B-phase, as shown in Fig. 13(a).

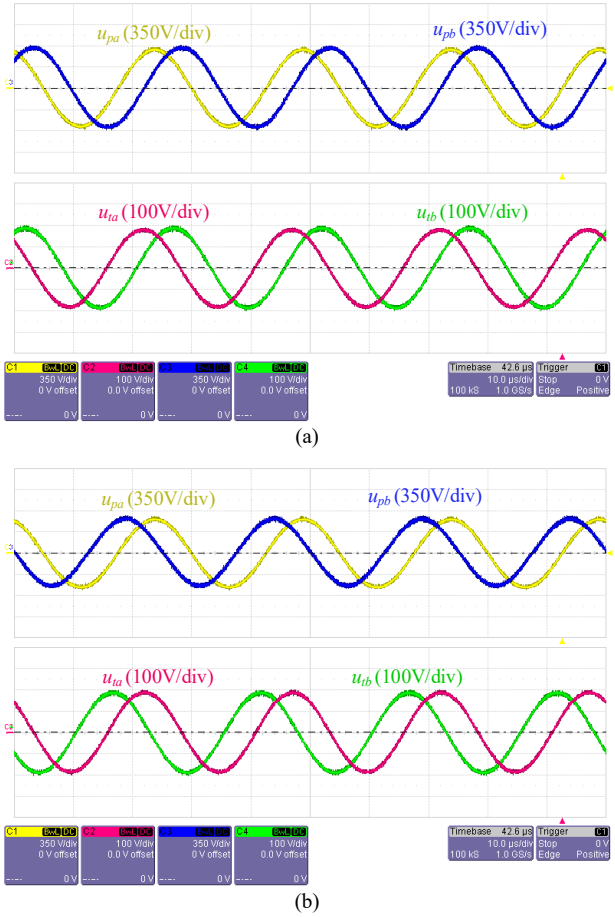

Fig. 13. Measured waveforms of bidirectional motion. (a) Forward motion. (b) Backward motion.

On the other hand, the rotor will rotate counterclockwise for backward motion when the B-phase voltage is ahead of the A-phase, as shown in Fig. 13(b). The bidirectional operation capability of the proposed wireless drive system can be readily implemented at the primary side without supplementary circuits, power switches and communication modules.

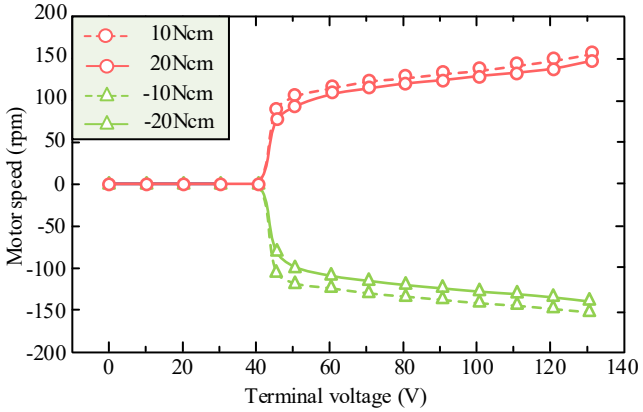

Fig. 14. Measured bidirectional speed characteristics with different loads.

To evaluate various scenarios of the motor operation, Fig. 14 shows the measured bidirectional speed characteristics versus different terminal voltages under different load conditions. The motor speed can be controlled from 89 to 156 rpm at a 10 Ncm load and adjustable between 76 and 148 rpm at the load torque of 20 Ncm. The motor speed is proportional to the motor terminal voltage within a certain range, which is due to the vibration of the piezoelectric elements being enhanced with the increase of the excitation voltage. Therefore, the experiment results well confirm the bidirectional motion capability of the proposed wireless USM.

C. Verification of Dual-Mode Wireless Drive Control

Flexible speed regulation is the key to wireless drives. Therefore, the wireless self-direct drive of the proposed system is evaluated as shown in Fig. 16, where the measured waveforms are the inverter outputs u_{ia} and u_{ib}, and motor terminal voltages u_{ta} and u_{tb}. In the high-speed region, the motor speed can be readily controlled and regulated by adjusting the value of δ_{WSDD}. Fig. 15(a) shows the situation when δ_{WSDD} = 1 (N_1 = 1 and N_2 = 0), which means that the motor speed is only regulated by the resonant frequency f_1 with the maximum speed. Accordingly, Fig. 15(b) shows the case of δ_{WSDD} = 4/5 (N_1 = 7 and N_2 = 1), where the motor speed drops as the input voltage of the motor terminal decreases.

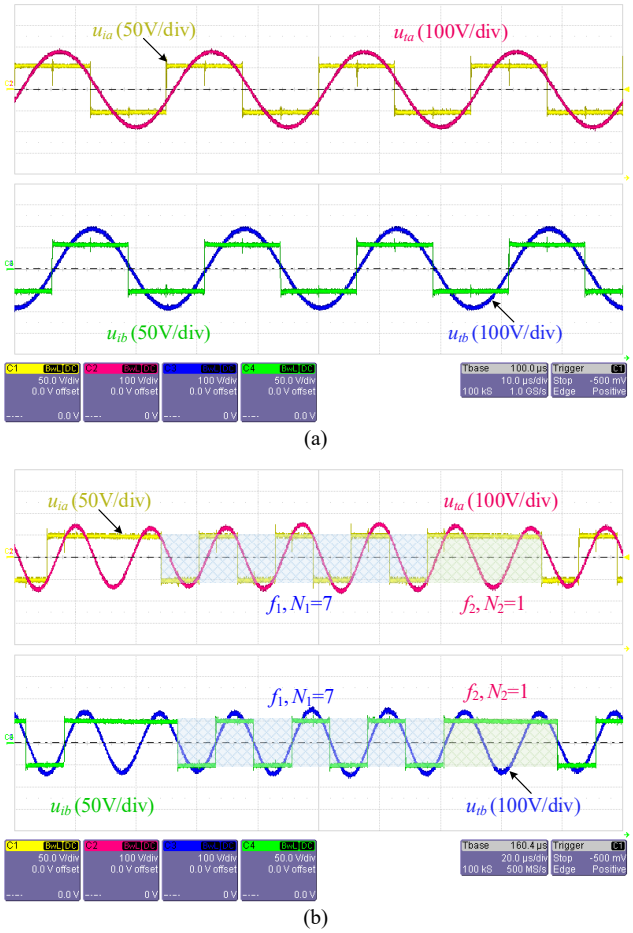

Fig. 15. Measured waveforms of wireless self-direct drive. (a) δ_{WSDD} = 1 (N_1 = 1 and N_2 = 0). (b) δ_{WSDD} = 4/5 (N_1 = 7 and N_2 = 1).

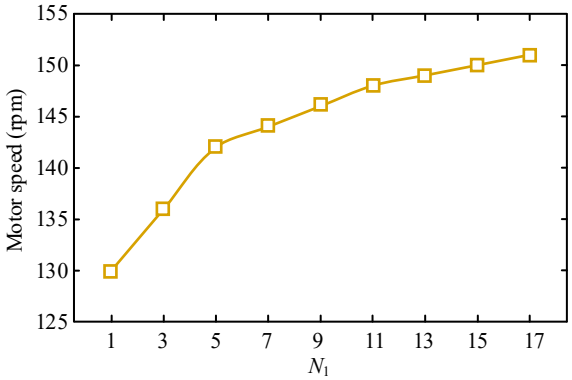

Fig. 16. Measured characteristics of WSDD control in high-speed region.

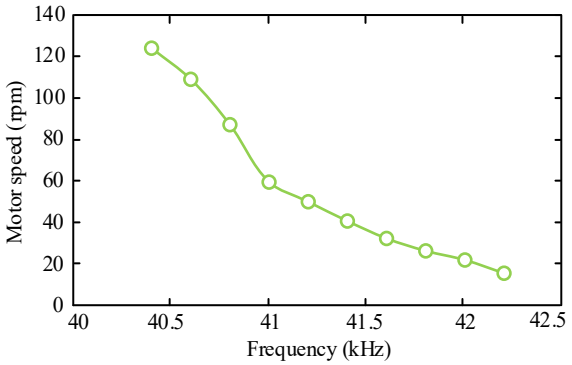

Fig. 17. Measured characteristics of VF control in low-speed region.

Furthermore, the measured motor speed over a wide range of variable δ_{WSDD} is tested as shown in Fig. 16. For simplicity, N_2 is set to the constant 1, adjusting N_1 from 1 to 17, while δ_{WSDD} is varied from 1/2 to 9/10. It can be observed that the motor speed increases gradually with the increase of N_1, which means that by adjusting the ratio of N_1 and N_2, the motor speed can be flexibly controlled, thus verifying the feasibility of the developed WSDD control for the wireless direct drive in the high-speed region. In addition, Fig. 17 shows the performance in the low-speed region with VF control. With the driving frequency increases, the motor speed can be well controlled in the low-speed region, thus overcoming the problem of the low-speed dead zone. The experimental results verify the feasibility of the proposed dual-mode wireless drive scheme for speed regulation in the full-speed range.

D. Verification of High-Robustness

Fig. 18 shows the measured waveforms of the inverter outputs u_{ia} and u_{ib}, and motor terminal voltages u_{ta} and u_{tb} of the proposed wireless drive system in the case of the variation in the coupling capacitance of the coupling mechanism. It can be observed that when the coupling capacitance varied from 830 pF to 680 pF, the terminal voltage drops slightly with a variation of 3.1%, and the motor speed is almost stable at around 162 rpm. The measured results show that the motor speed is less affected by the coupling capacitance within a certain degree, which well confirms the obvious advantages of the proposed wireless drive system being insensitive to the coupling mechanism and overcomes the shortcomings of the insufficient robustness of previous wireless motors.

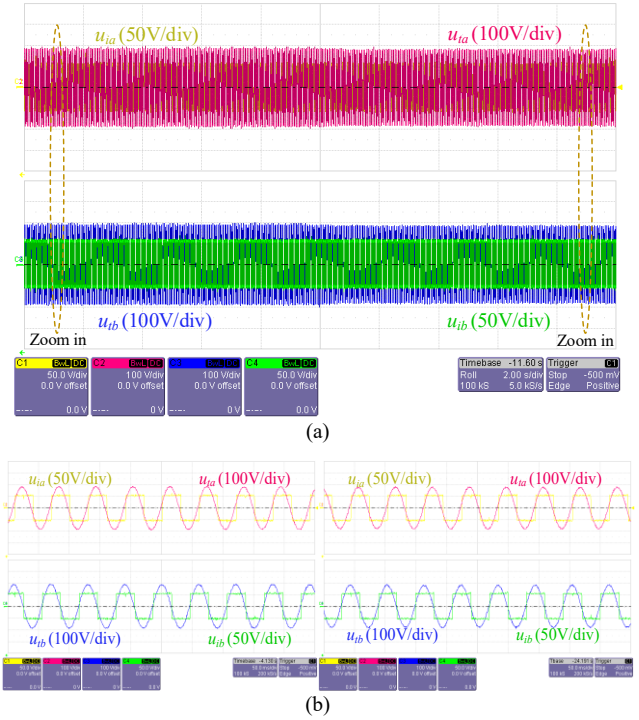

Fig. 18. Measured waveforms. (a) Full view. (b) Zoom-in view with 830 pF coupling capacitance (left) and 680 pF coupling capacitance (right).

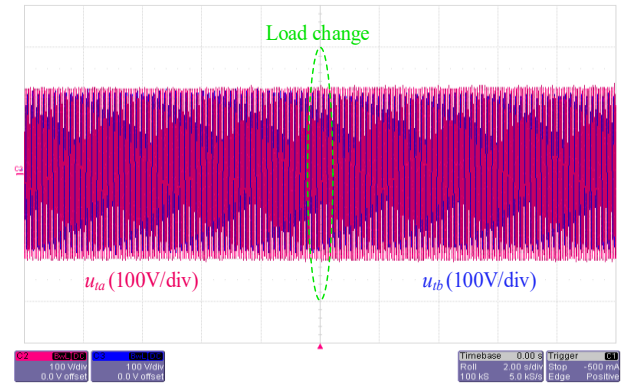

Fig. 19. Measured waveforms of load changes.

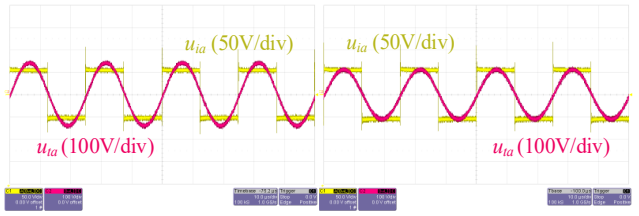

Fig. 20. Measured waveforms with no variation in compensation capacitor (left) and 6% variation (right).

In addition, to comprehensively demonstrate the robustness of the system, Fig. 19 and Fig. 20 show the measured waveforms for the variation of the system load and secondary-side compensation capacitors, respectively. Fig. 19 demonstrates the robustness of the system to load variations, where the load is increased abruptly from no load to 20 Ncm. The measured motor terminal voltages are very stable with an insignificant variation of 1.33% only, which ensures the stability of USM operation. Fig. 20 shows the measured waveforms before and after a 6% reduction in the secondary-side compensation capacitors, and the results show that the change of compensation capacitor parameters will slightly affect the amplitude of motor terminal voltages. However, according to the voltage speed characteristics of the USM, the fluctuation of the motor speed is much smaller than those of the terminal voltages. Thus, the reliability of the USM operation is guaranteed to a certain extent. Meanwhile, it is recommended that the compensation capacitors should be packaged and maintained regularly in practical applications to minimize the influence of capacitor parameter variations.

E. Discussion and Recommendation

To highlight the innovation and superiority of the proposed wireless drive system, a comprehensive comparison with the existing wireless motor systems is summarized and analyzed in Table II.

It can be observed that all the secondary sides of existing wireless motors are unreliable. Wireless DC motors suffer from carbon brush wear, while wireless SPIM requires numerous power switches at the motor side. Wireless SRMs and wireless stepping motors are without the need for active power switches, but communication devices such as Bluetooth and rectifiers are necessary, which inevitably reduce the reliability of the system. In addition, the bidirectional motion capabilities of the existing wireless motors are not fully developed, as most systems require complex peripheral circuits or bulky multi-frequency WPT, thereby reducing the simplicity and integrability of the system. Moreover, all of them are susceptible to coupling mechanism misalignment, which inevitably degrades the stability of the system and is not conducive to practical applications, .

On the contrary, the proposed wireless USM system exhibits distinct novelty and superiority over existing wireless motor systems, as summarized below.

1. Eliminating the utilization of secondary-side active power switches, rectifiers and communication modules, which is more conducive to high-degree integration.
2. Bidirectional motion capability and full-speed range regulation can be readily achieved without the involvement of complex peripheral circuits, realizing the true sense of wireless self-direct drive.
3. Strong robustness with insensitivity to coupling mechanism misalignment is naturally obtained, which improves reliability and facilitates stable operation in complex environments.
4. The inherent magnetic-free characteristics avoid strong magnetic field interference and are promising for biomedical applications.

For practical applications, the transmission power of the CPT system can meet the power requirements of biomedical applications as shown in Table II. In addition, a high transmission efficiency from power supply to motor terminal is achieved, which is attributed to the proposed system eliminating the inverter and power switches at the secondary side, thereby reducing the switching and conduction losses.

TABLE II
COMPARISON OF EXISTING WIRELESS MOTOR SYSTEMS AND PROPOSED WIRELESS USM

Ref.	Resonant frequencies	Motor types	Bidirectional motions	Secondary switches	Communication modules	Coupler sensitivity	Transmission power	System efficiency	Recommendations
[10]	Two	DC	√	12	0	High	N/A	85%	√√
[11]	Two	SPIM	×	33	0	High	110 W	86.2%	√
[13]	Three	SRM	√	12	1	High	N/A	72.8%	√
[15]	Single	SRM	√	12	1	High	134.87 W	89.1%	√√
[16]	Single	Stepping	√	16	1	High	N/A	87.5%	√√
Proposed	Single	USM	√	0	0	Low	23.9 W	87.2%	√√√

N/A: Not available

VI. CONCLUSION

In this paper, a magnet-free wireless self-direct drive USM system has been proposed and implemented. The proposed wireless USM takes definite advantages over the existing wireless motors in terms of simplicity, controllability, and high-robustness. Specifically, the proposed wireless motor can be directly driven by the secondary compensation network without the need for active or passive power switches at the motor side. Meanwhile, the precise servo motion can be easily realized as the full-speed range bidirectional motion capabilities can be fully developed by using the proposed dual-mode wireless drive control, without the need for cumbersome extra circuitry or selective WPT. More importantly, the inherent insensitivity to the misalignment of the coupling mechanism enables the proposed system highly reliable and robust under complex operating conditions. The feasibility of the proposed wireless drive system is verified by theoretical analysis and hardware experimentation. Prominently, this work validates the seamless integration between high-frequency WPT and USMs, offering broad prospects for future miniaturization and biomedical implantation.

REFERENCES

[1] Z. Zhang, H. Pang, A. Georgiadis, and C. Cecati, "Wireless power transfer—an overview," *IEEE Trans. Ind. Electron.*, vol. 66, no. 2, pp. 1044–1058, Feb. 2019.

[2] H. Zhang and F. Lu, "An improved design methodology of the double-sided LC-compensated CPT system considering the inductance detuning," *IEEE Trans. Power Electron.*, vol. 34, no. 11, pp. 11396–11406, Nov. 2019.

[3] Y. Liu, C. Liu, S. Liu, and Y. Huang, "Design and control of a novel wireless energy router with independent power transmission channels," *IEEE Trans. Power Electron.*, vol. 38, no. 3, pp. 2940-2955, Mar. 2023.

[4] C. C. Mi, G. Buja, S. Y. Choi, and C. T. Rim, "Modern advances in wireless power transfer systems for roadway powered electric vehicles," *IEEE Trans. Ind. Electron*., vol. 63, no. 10, pp. 6533–6545, Oct. 2016.

[5] Y. Wang, H. Zhang, and F. Lu, "3.5-kW 94.2% DC–DC efficiency capacitive power transfer with zero reactive power circulating," *IEEE Trans. Power Electron.*, vol. 38, no. 2, pp. 1479–1484, Feb. 2023.

[6] C. Xiao, D. Cheng, and K. Wei, "An LCC-C compensated wireless charging system for implantable cardiac pacemakers: Theory, experiment, and safety evaluation," *IEEE Trans. Power Electron.*, vol. 33, no. 6, pp. 4894-4905, Jun. 2018.

[7] C. Li, Z. Wang, and Y. Xu, "A wireless-power-transfer-based three-phase PMSM drive system with matrix converter," *IEEE Trans. Ind. Electron.*, vol. 70, no. 3, pp. 2307–2317, Mar. 2023.

[8] H. Liu, H. Zhou, Q. Deng, W. Hu, X. Gao, and L. Fang, "A wireless DC motor drive using LCCC-CCL compensated network with bidirectional motion capability," *IEEE Trans. Circuits Syst. I, Reg. Papers*, vol. 69, no. 11, pp. 4714–4725, Nov. 2022.

[9] M. Sato, G. Yamamoto, D. Gunji, T. Imura, and H. Fujimoto, "Development of wireless in-wheel motor using magnetic resonance coupling," *IEEE Trans. Power Electron.*, vol. 31, no. 7, pp. 5270–5278, Jul. 2016.

[10] C. Jiang, K. T. Chau, C. H. T. Lee, W. Han, W. Liu, and W. H. Lam, "A wireless servo motor drive with bidirectional motion capability," *IEEE Trans. Power Electron.*, vol. 34, no. 12, pp. 12001–12010, Mar. 2019.

[11] H. Wang, K. T. Chau, C. H. T. Lee, L. Cao, and W. H. Lam, "Design, analysis, and implementation of wireless shaded-pole induction motors," *IEEE Trans. Ind. Electron.*, vol. 68, no. 8, pp. 6493–6503, Aug. 2021.

[12] H. Wang, K. T. Chau, C. H. T. Lee, and C. Jiang, "Wireless shaded-pole induction motor with half-bridge inverter and dual-frequency resonant network," *IEEE Trans. Power Electron.*, vol. 36, no. 12, pp. 13536–13545, Dec. 2021.

[13] C. Jiang, K. T. Chau, C. Liu, and W. Han, "Design and analysis of wireless switched reluctance motor drives," *IEEE Trans. Ind. Electron.*, vol. 66, no. 1, pp. 245–254, Jan. 2019.

[14] Z. Gu, J. Wang, Z. Liang, Y. Wu, C. Cecati, and Z. Zhang, "Single-transmitter multiple-pickup wireless power transfer: Advantages, challenges, and corresponding technical solutions," *IEEE Ind. Electron. Mag.*, vol. 14, no. 4, pp. 123–135, Dec. 2020.

[15] W. Han, K. T. Chau, Z. Hua, and H. Pang, "An integrated wireless motor system using laminated magnetic coupler and commutative-resonant control," *IEEE Trans. Ind. Electron.*, vol. 69, no. 5, pp. 4342–4352, May 2022.

[16] Y. Chen, C. Gan, H. Shi, K. Ni, and R. Qu, "Design of wireless individual-drive system for variable reluctance stepping motor," *IEEE Trans. Circuits Syst. II Exp. Briefs*, vol. 69, no. 4, pp. 2141–2145, Apr. 2022.

[17] K. Li, W. Ding, J. Yuan, and C. Du, "A decoupled multichannel based wireless SRM system with tunable compensation network and multifrequency pulse density control," *IEEE Trans. Ind. Electron.*, Early Access, 2023, doi: 10.1109/TIE.2023.3250748.

[18] Z. Yuan, M. Saeedifard, C. Cai, Q. Yang, P. Zhang, and H. Lin, "A misalignment tolerant design for a dual-coupled LCC-S-compensated WPT system with load-independent CC output," *IEEE Trans. Power Electron.*, vol. 37, no. 6, pp. 7480–7492, Jun. 2022.

[19] L. Hofstetter et al., "MRI-compatible electromagnetic servomotor for image-guided medical robotics," *Commun Eng.*, vol. 1, no. 1, p. 4, Dec. 2022.

[20] C. Jiang, K. T. Chau, C. Liu, and W. Han, "Wireless DC motor drives with selectability and controllability," *Energies*, vol. 10, no. 1, p. 49, Jan. 2017.

[21] K. Lu, X. Li, Y. Zhao, P. Yi, B. Yan, and W. Hua, "A novel three-vector-based model predictive flux control with low computation complexity for SPMSM," *IEEE Trans. Transport. Electrific*., doi: 10.1109/TTE.2023.3315522.

[22] H. Jin et al., "Review on piezoelectric actuators based on high-performance piezoelectric materials," *IEEE Trans. Ultrason., Ferroelectr., Freq. Control*, vol. 69, no. 11, pp. 3057–3069, Nov. 2022.

[23] Y. Liu, W. Chen, J. Liu, and X. Yang, "A high-power linear ultrasonic motor using bending vibration transducer," *IEEE Trans. Ind. Electron.*, vol. 60, no. 11, pp. 5160-5166, Nov. 2013.

[24] F. Lu, H. Zhang, H. Hofmann, and C. C. Mi, "A double-sided LC compensation circuit for loosely coupled capacitive power transfer," *IEEE Trans. Power Electron.*, vol. 33, no. 2, pp. 1633–1643, Feb. 2018.

[25] B. Luo, R. Mai, L. Guo, D. Wu, and Z. He, "LC–CLC compensation topology for capacitive power transfer system to improve misalignment performance," *IET Power Electron.,* vol. 12, no. 10, pp. 2626–2633, Aug. 2019.

[26] X. Dai, M. Sun, P. Deng, R. Wang, and Y. Su, "Asymmetric bidirectional capacitive power transfer method with push–pull full-bridge hybrid topology," *IEEE Trans. Power Electron.*, vol. 37, no. 11, pp. 13902–13913, Nov. 2022.

[27] Y. Xiao, Y. Yang, C. Liu, and J. Rodriguez, "Design and analysis of a wireless ultrasonic motor drive system," *IEEE Trans. Power Electron.*, vol. 38, no. 10, pp. 12309-12314, Oct. 2023.
[28] W. Liu, K. T. Chau, C. H. T. Lee, W. Han, X. Tian, and W. H. Lam, "Full-range soft-switching pulse frequency modulated wireless power transfer," *IEEE Trans. Power Electron.*, vol. 35, no. 6, pp. 6533–6547, Jun. 2020.
[29] Z. Hua, K. T. Chau, W. Han, W. Liu, and T. W. Ching, "Output-controllable efficiency-optimized wireless power transfer using hybrid modulation," *IEEE Trans. Ind. Electron.*, vol. 69, no. 5, pp. 4627–4636, May 2022.

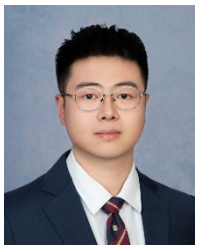

Zhiwei Xue (Graduate Student Member, IEEE) is currently working toward the Ph.D. degree in electrical and electronic engineering with the Department of Electrical and Electronic Engineering at the University of Hong Kong, Hong Kong, China. From 2021 to 2022, he was a Research Assistant at the Department of Electrical Engineering, The Hong Kong Polytechnic University, Hong Kong, China.

His research interests include wireless power transfer, electrical machine drives, power electronics, and electric vehicle technologies.

K. T. Chau (Fellow, IEEE) received the B.Sc. (Eng.), M.Phil., and Ph.D. degrees in electrical and electronic engineering from The University of Hong Kong, Hong Kong, in 1988, 1991, and 1993, respectively. Currently, he serves as Chair Professor of Electrical Energy Engineering at the Research Centre for Electric Vehicles and Department of Electrical and Electronic Engineering, The Hong Kong Polytechnic University. His research interests include electric and hybrid vehicles, power electronics and drives, and renewable energies. He is the author of nine books and more than 350 journal papers.

Prof. Chau is a Fellow of the Institution of Engineering and Technology (IET), U.K., and of the Hong Kong Institution of Engineers. He is also a Co-editor of the Journal of Asian Electric Vehicles. He is a Chartered Engineer. He was the recipient of the Changjiang Chair Professorship from the Ministry of Education, China, and the Environmental Excellence in Transportation Award for Education, Training, and Public Awareness from the Society of Automotive Engineers International.

Wei Liu (Member, IEEE) received the B.Eng. and M.Eng. degrees in electrical engineering from China University of Petroleum, Qingdao, China, and a Ph.D. degree in electrical and electronic engineering from The University of Hong Kong (HKU), Hong Kong, China, in 2014, 2017, and 2021, respectively.

He is currently an Assistant Professor at the Research Centre for Electric Vehicles and Department of Electrical and Electronic Engineering, The Hong Kong Polytechnic University (PolyU). He served as a Postdoctoral Fellow and then was promoted to Research Assistant Professor at the Department of Electrical and Electronic Engineering, HKU from 2021 to 2023. He also worked as a Visiting Researcher with Nanyang Technological University, Singapore (NTU), in 2019. His research interests include wireless power transfer, power electronics, biomedical power electronics, and electric vehicle technologies.

Dr. Liu was the recipient of the Power Engineering Prize from HKU, the Excellent Paper Award, and the Best Presentation Award from international conferences in the area of Electric Vehicles and Transportation Electrification. He is also a Guest Associate Editor of *IEEE Journal of Emerging and Selected Topics in Power Electronics (JESTPE)*, Guest Editor of international journals, and Session Chair of international conferences.

Zhichao Hua (Member, IEEE) received the B.Eng. degree in electrical engineering and automation from Wuhan University of Technology, Wuhan, China, in 2016 and the M.Eng. degree in electrical and electronic engineering from Huazhong University of Science and Technology, Wuhan, China, in 2019, respectively, and the Ph.D. degree in electrical and electronic engineering from The University of Hong Kong, Hong Kong, China, in 2023.

His research interests include power electronics, wireless power transfer techniques, and electric vehicle technologies.